UDC 621.3 https://doi.org/10.20998/2074-272X.2024.4.04

Ch. Sajan, P. Satish Kumar, P. Virtic

Enhancing grid stability and low voltage ride through capability using type 2 fuzzy controlled dynamic voltage restorer

Introduction. *The integration of Renewable Energy Sources (RESs), particularly Wind Energy Conversion Systems (WECS), is vital for reducing reliance on fossil fuels and addressing climate change. However, this transition poses challenges, including ensuring grid stability in the face of intermittent RESs. Compliance with grid codes is crucial, with a focus on Low Voltage Ride Through (LVRT) capability.* ***Problem.*** *The intermittent nature of RESs, specifically in Permanent Magnet Synchronous Generator (PMSG) based WECS, presents challenges to grid stability during voltage dips.* ***Goal.*** *To enhance voltage stability and LVRT capability in PMSG-based WECS by integrating a Dynamic Voltage Restorer (DVR) with an energy storage device. This involves regulating the input DC voltage to the DVR using a type 2 fuzzy controller, adapting intelligently to changing conditions.* ***Methodology.*** *DVR, powered by an energy storage device, is strategically integrated with WECS. A type 2 fuzzy controller regulates the DC voltage to DVR. The rectified WECS output undergoes processing through an isolated flyback converter. A 31-level Cascaded H-Bridge Multilevel Inverter (CHBMLI) with PI control ensures high-quality AC output.* ***Results.*** *The validation of developed system is executed using MATLAB/Simulink revealing a reduced Total Harmonic Distortion (THD) value of 1.8 %, ensuring significance in LVRT capability.* ***Originality.*** *The strategic integration of DVR with PMSG-based WECS, addresses the LVRT challenges. The use of type 2 fuzzy controller for intelligent voltage regulation and a sophisticated multilevel inverter contributes to the uniqueness of proposed solution.* ***Practical value.*** *The developed system provides benefits by ensuring reliable LVRT capability in PMSG-based WECS with reduced THD of 1.8 % indicating improved grid compatibility.* References 26, tables 5, figures 20.

Key words: **permanent magnet synchronous generator, wind energy conversion systems, low voltage ride through, type 2 fuzzy controller, isolated flyback converter, 31-level cascaded H-bridge multilevel inverter, PI controller.**

Вступ. *Інтеграція відновлюваних джерел енергії (RESs), особливо систем перетворення енергії вітру (WECS), має життєво важливе значення для зниження залежності від викопного палива та вирішення проблеми зміни клімату. Однак цей перехід створює проблеми, у тому числі забезпечення стабільності мережі в умовах уривчастої роботи RESs. Дотримання мережевих норм має вирішальне значення, при цьому особлива увага приділяється можливості роботи при низькій напрузі (LVRT).* ***Проблема***. *Уривчастий характер RESs, особливо в WECS на основі синхронного генератора з постійними магнітами (PMSG), створює проблеми для стабільності мережі під час провалів напруги.* ***Мета***. *Підвищити стабільність напруги та можливості LVRT у WECS на базі PMSG за рахунок інтеграції динамічного відновника напруги (DVR) із пристроєм зберігання енергії. Це передбачає регулювання вхідної постійної напруги на DVR за допомогою нечіткого контролера типу 2, що інтелектуально адаптується до умов, що змінюються.* ***Методологія***. *DVR, який працює від накопичувача енергії, стратегічно інтегрований із WECS. Нечіткий контролер типу 2 регулює напругу постійного струму, що подається на DVR. Випрямлений вихідний сигнал WECS проходить обробку через ізольований зворотноходовий перетворювач. 31-рівневий каскадний багаторівневий інвертор H-Bridge (CHBMLI) із ПІ-регулюванням забезпечує високоякісний вихід змінного струму.* ***Результати***. *Валідація розробленої системи виконується з використанням MATLAB/Simulink, демонструючи зменшене значення загального гармонічного спотворення (THD) 1,8 %, що забезпечує важливість можливостей LVRT.* ***Оригінальність***. *Стратегічна інтеграція DVR із WECS на базі PMSG вирішує проблеми LVRT. Використання нечіткого контролера 2-го типу для інтелектуального регулювання напруги та складного багаторівневого інвертора сприяє унікальності запропонованого рішення.* ***Практична цінність***. *Розроблена система забезпечує переваги, забезпечуючи надійну роботу LVRT у WECS на базі PMSG зі зниженим THD на 1,8 %, що вказує на покращену сумісність із мережею.* Бібл. 26, табл. 5, рис. 20.

Ключові слова: **синхронний генератор з постійними магнітами, системи перетворення енергії вітру, прохідність низької напруги, нечіткий контролер типу 2, ізольований зворотноходовий перетворювач, 31-рівневий каскадний багаторівневий інвертор Н-мосту, ПІ-регулятор.**

Abbreviations

CHBMLI	Cascaded H-Bridge Multilevel Inverter	STATCOM	Static Synchronous Compensator
DVR	Dynamic Voltage Restorer	SVC	Static Var Compensator
ESD	Energy Storage Device	THD	Total Harmonic Distortion
LVRT	Low Voltage Ride Through	T2-FLC	Type 2 Fuzzy Logic Controller
PMSG	Permanent Magnet Synchronous Generator	VSI	Voltage Source Inverter
PCC	Point of Common Coupling	VUF	Voltage Unbalance Factor
PWM	Pulse Width Modulator	WECS	Wind Energy Conversion Systems
RES	Renewable Energy Source	WT	Wind Turbines

Introduction. The adoption of wind power has experienced rapid growth, evident from the surge in wind farm installations. In 2018 alone, 51.3 GW of wind energy capacity was added, contributing to a significant total installed capacity of 591 GW by that year. Wind power stands out as a sustainable and eco-friendly energy source, offering the advantage of offshore installations to conserve land resources [1]. Despite these benefits, the expanding presence of wind power raises concerns about the stability of the power grid. Consequently, there is a pressing need for more stringent grid regulations to ensure the incorporation of wind power systems without compromising the existing grid's reliability and stability [2].

As wind power integration expands, grid stability becomes crucial. PMSG WTs offer superior control. Unlike doubly fed induction generator [3] turbines, PMSG turbines have a broader operational range using advanced converters. The key advantage of PMSG WTs lies in their wide operational range, leveraging power converters like machine-side converters and grid-side converters to their fullest extent [4]. To regulate power

flow in PMSG-WECS during unbalanced conditions, back-to-back converters are essential [5]. These converters help maintain stable voltages, particularly during asymmetrical faults. Due to the nonlinear nature of wind farms, automated control strategies are crucial [6].

Numerous techniques have been suggested to mitigate fluctuations in wind power. In prior studies, researchers [7] focused on pitch angle control, aiming to achieve stable output power levels and minimize flicker. Another approach explored the utilization of indirect field oriented control for power smoothing [8]. However, these methods have limitations in terms of control range due to reduced wind power acquisition. PMSG is highly susceptible to grid voltage disturbances, leading to issues such as rotor over-current, excessive DC-link voltage, and torque oscillations during grid faults. These problems impact the drive's lifespan. To enhance LVRT capability of PMSG-WECS, various solutions have been suggested that are broadly categorized as software-based and hardware-based [9]. Table 1 summarizes some of the hardware and software based solution with their challenges.

Table 1

Summary of existing solution

Solution	Advantages	Challenges	Solutions proposed
Software based solution			
Demagnetizing control [10]	Suitable for Moderate faults	Limited effectiveness during severe grid faults	DVR with type 2 fuzzy overcomes limited effectiveness during severe grid faults
Flux linkage tracking control [11]	Enhanced stability and better fault detection	Increased computational load and limited to specific grid conditions	Fuzzy logic controllers are known for their ability to handle uncertainties and variations without requiring precise mathematical models, potentially leading to a more computationally efficient solution
Partial feedback linearization control [12]	Improved response time with enhanced grid integration	Complexity in implementation and requires precise modeling of system dynamics	Type 2 fuzzy logic, are known for their ability to handle uncertainties and variations in a flexible manner thereby facilitating reduced computational complexity
Hardware based solution			
Fault current limiter [13]	High fault tolerance	Expensive technology and maintenance challenges	Reduces the need for constant fine-tuning and adjustment which is beneficial for maintenance
Crowbar and chopper scheme [14]	Quick response to faults	Disruptive to grid during activation and limited effectiveness for prolonged faults	In the context of prolonged faults, the type 2 fuzzy controller could intelligently adjust the control parameters to maintain optimal performance, ensuring sustained effectiveness
Series grid-side converter [15]	Provides grid support and effective for unbalanced faults	Requires precise control	Type 2 fuzzy controller intelligently regulates the input DC voltage to the DVR, adapting to the dynamic and changing conditions that may occur during grid faults which is crucial in scenarios where precise control would be difficult

Flexible AC transmission system technology, utilizing power electronics, addresses power industry challenges. Devices like STATCOM [16] and SVC [17] come in series, shunt, and hybrid connections. STATCOM supplies reactive power to regulate voltage at PCC, while SVC enhances system stability. However, drawbacks include high cost, complexity, and grid-specific effectiveness, making implementation challenging for some utilities. As a consequence, DVR [18] is implemented in the proposed work, to compensate for LVRT and maintain a stable voltage supply to sensitive loads. When voltage sags occur due to faults or disturbances in the grid, the DVR detects sag and injects compensating voltage, restoring power quality to connected equipment.

These protective methods enhance LVRT performance to some extent. However, without an ESD, WTs are unable to regulate output power fluctuations effectively. Alternatively, ESDs have been widely considered [19, 20], for smooth active power fluctuations but also regulate reactive power. In such a way, DVRs are connected in series with the load and coupled with ESD, transformer, and inverter. These components compensate for active and reactive power needs during voltage fluctuations [21]. DVRs stabilize voltages by injecting compensating voltage into the distribution system via a transformer. In [22] optimized PI control with a gradient adaptive variable learning rate Least Mean Square algorithm is developed to ensure adaptability by adjusting step sizes, making it robust in dynamic system conditions. Still, optimizing and implementing adaptive algorithms, require significant computational resources and could add complexity to system. Levenberg Marquardt back-propagation algorithm, and Adaptive Neuro-Fuzzy Inference System model in [23] shows improved accuracy and power quality responses. However, potential challenges include the complexity of implementing advanced artificial intelligence techniques, requiring expertise, and the computational resources. Addressing these research gaps would provide a more exact understanding of the challenges and opportunities in enhancing LVRT capabilities in PMSG-wind energy systems, leading to more effective and reliable grid integration solutions. Therefore, the main purpose of this work is to address the challenges associated with the integration of RESs, specifically focusing on the intermittent nature of PMSG based WECS. The primary goal is to enhance grid stability and LVRT capability by proposing a solution that strategically integrates a DVR with an ESD. The innovative use of a type 2 fuzzy controller for intelligent regulation of the DVR's input DC voltage, coupled with a sophisticated 31-Level CHBMLI, aims to ensure high-quality AC output and reduced THD, ultimately providing a practical and reliable system for improved grid compatibility and stability in PMSG based WECS. The key contributions of the work include:

- Integrates DVR with supercapacitor to enhance LVRT capability of WECS.

• Implements type 2 fuzzy controller for precise and adaptive control of DVR, ensuring stable responses to voltage fluctuations and grid disturbances.

• Incorporates DVR, isolated flyback converter, and reduced switch 31-Level CHBMLI controlled by PI controller for seamless power flow and high-quality AC output.

Description of proposed work. The goal of this research is to address the challenges associated with integrating RESs, particularly WECS, into the modern power grid (Fig. 1). The focus lies on enhancing LVRT capability, crucial for maintaining grid stability in the presence of intermittent and variable RESs. This has been achieved through the strategic integration of key components.

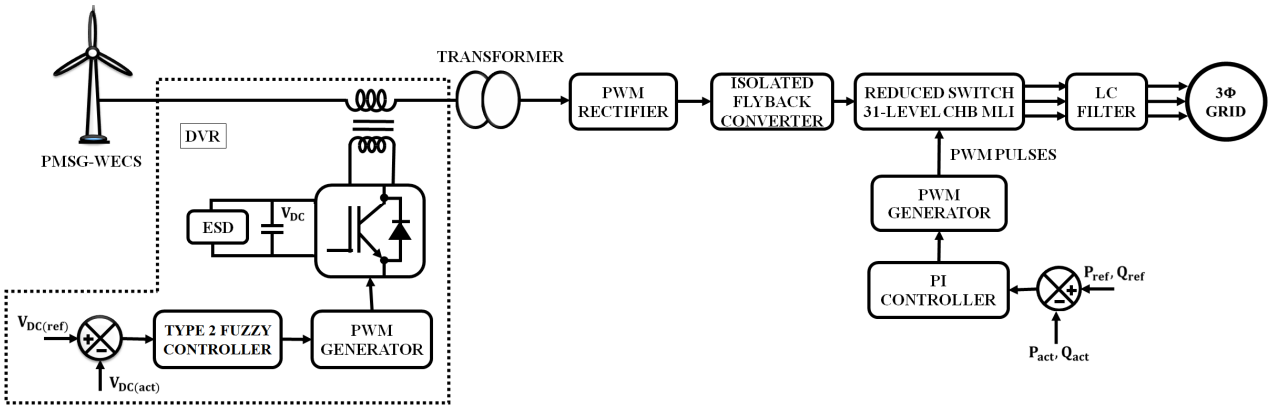

Fig. 1. Proposed PMSG-WECS with DVR

The proposed system is an intricate and efficient solution for integrating wind energy into power grid, ensuring grid stability, even during voltage dips and disturbances. It begins with a WECS equipped with a PMSG that captures wind energy and transforms it into electrical power. To tackle situations of LVRT, the system seamlessly activates DVR linked to a supercapacitor acting as an ESD. This combination ensures a continuous supply of stable AC power to the grid, mitigating voltage fluctuations. Crucially, a type 2 fuzzy controller regulates the input voltage to DVR, adapting to dynamic grid conditions. To refine the power output, the system utilizes a transformer to step up the voltage and PWM rectifier to convert the AC supply into DC, which is directed to an isolated flyback converter. This converter adjusts voltage levels and ensures electrical isolation. The regulated output from flyback converter is then fed into 31 CHBMLI. This advanced inverter converts DC into AC power by creating multiple voltage levels, minimizing harmonics and voltage variations in output. To ensure precision control, the PI controller at the grid side continuously monitors real and reactive power, generating control signals for 31-level CHBMLI. These signals adjust the inverter's operation, maintaining the required voltage and frequency, facilitating efficient and reliable grid synchronization. The proposed LVRT solution with DVR surpasses existing systems by offering a combination of fast response times, continuous supply stability, adaptability, reduced voltage fluctuations, improved grid resilience, and a unified system integration approach.

Modelling of system components. PMSG-WT modelling. Modelling a PMSG-based WT is essential for understanding its dynamic behavior and optimizing performance. Figure 2 depicts the schematic representation of PMSG wind system.

Aerodynamic modelling. The PMSG based WT harnesses wind energy to produce mechanical power through the following mechanism:

$$P_W = \frac{1}{2}\rho A V_W^3 C_p(\lambda,\beta). \quad (1)$$

Here, the captured wind power P_W in the PMSG-WT is determined by power coefficient C_p, air density ρ, swept area A and wind velocity without rotor interference V_W^3. As shown in (1), the power coefficient of a WT is determined by the ratio of pitch angle β to tip speed λ:

$$C_p(\lambda,\beta) = c_1\left(\frac{c_2}{\lambda_i} - c_3\beta - c_4\right)e^{-c_5/\lambda_i} + c_6\lambda, \quad (2)$$

where

$$\frac{1}{\lambda_i} = \frac{1}{\lambda - 0.08\beta} - \frac{0.035}{\beta^3 + 1}, \quad (3)$$

and characteristics of wind are represented as c_1 – c_6, respectively.

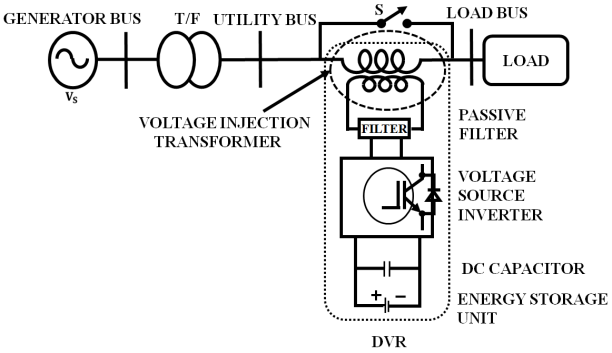

Fig. 2. DVR based scheme for LVRT improvement of PMSG

PMSG modelling. The dynamic model of PMSG WT employs *dq* reference rotating frame, expressed as:

$$\frac{d\psi_{sd}}{dt} = -V_{sd} - R_s I_{sd} - \omega_e \psi_{sq}; \quad (4)$$

$$\frac{d\psi_{sq}}{dt} = -V_{sq} - R_s I_{sq} - \omega_e \psi_{sd}. \quad (5)$$

From (4) and (5):

$$\psi_{sd} = (L_{sd} + L_{md})I_{sd} + \psi_m; \quad (6)$$

$$\psi_{sq} = (L_{sq} + L_{mq})I_{sq}, \quad (7)$$

where ψ_{sq}, ψ_{sd} are the stator flux linkages; L_{sq}, L_{sd} are the stator leakage inductances; L_{md}, L_{mq} refer to magnetizing

inductances; ψ_m is the linkage flux of the permanent magnet in the motor.

On solving the differential expression becomes

$$L_d \frac{\mathrm{d}I_{sd}}{\mathrm{d}t} = -V_{sd} - R_s I_{sd} - \omega_e L_q I_{sq}\,; \tag{8}$$

$$L_q \frac{\mathrm{d}I_{sq}}{\mathrm{d}t} = -V_{sq} - R_s I_{sq} - \omega_e L_d I_{sd} + \omega_e \psi_m\,; \tag{9}$$

$$P_s = V_{sd} I_{sd} + V_{sq} I_{sq}\,; \tag{10}$$

$$Q_s = V_{sq} I_{sd} - V_{sd} I_{sq}\,; \tag{11}$$

Enhancing LVRT by DVR technology. The DVR is essential for mitigating LVRT issues in renewable energy systems, especially PMSG-WECS. During grid faults, it swiftly detects voltage deviations and injects compensating voltage into the system. Continuous monitoring at the PCC allows the DVR to calculate and counteract voltage errors, ensuring rapid correction within milliseconds. Key elements like ESD, VSI and passive filters work together to manage voltage sags and harmonics, enhancing the resilience of power networks and minimizing disruptions to sensitive loads.

Energy storage device. ESD within a DVR incorporates various storage devices, in the proposed work it is supercapacitor. Its primary function is to provide essential real power during instances of voltage sags. DVR's compensating ability depends on ESD's quick charging and draining response times, where the rate of discharge determines how much internal space is set aside for energy storage.

Voltage source inverter. The pulse-width modulated VSI is responsible for converting DC voltage sourced from the ESD into AC voltage. This converted AC voltage is then supplied to the series transformer, which acts as a step-up voltage injection transformer. The series transformer elevates the voltage to effectively counteract conditions of voltage sag. Notably, the VSI operates with minimal voltage output, and for DVR protection, a bypass switch is commonly integrated.

Passive filters. To address the high-frequency harmonic in output of VSI, DVRs are equipped with passive filters. When positioned on inverter side, passive filters notably reduce stress on injection transformer. Simultaneously, when placed on the load side, they minimize harmonic content originating from transformer's secondary side. This integration of passive filters contributes to enhanced system performance and stability by mitigating the impact of harmonic distortions in DVR's output.

The DVR integrated in the line between PMSG and grid, enhances PMSG's LVRT capability. Capable of mitigating voltage fluctuations, including swells, sags, and harmonics, the DVR is particularly effective in compensating for voltage sag incidents in LVRT applications of PMSG. Figure 2 illustrates the installation of DVR at PCC, where it injects series voltage to compensate for active and reactive power in grid, aiding recovery from faults.

The injected series voltage by the DVR is expressed as:

$$V_{DVR} = V_L + Z_{TH} I_L - V_{TH}\,, \tag{12}$$

where I_L is the load current; V_L is the load voltage; Z_{TH} is the load impedance; V_{TH} is the system voltage during fault. The expression for load current is:

$$I_l = \frac{P_L + jQ_L}{V}\,. \tag{13}$$

On considering V_L as a reference, the equation is reformulated as:

$$V^*_{DVR} = V_L^{\angle 0} + Z_{TH}^{\angle(\beta-\theta)} - V_{TH}^{\angle\delta}\,, \tag{14}$$

where

$$\theta = \tanh^{-1}\left(\frac{\theta_L}{P_L}\right). \tag{15}$$

The expression for DVR's complex power output is:

$$S_{DVR} = V_{DVR} \cdot I^*_{DVR}\,. \tag{16}$$

The DVR's power rating is determined by magnitude of fault voltage to be compensated, and relationship provided calculates required active power of the DVR (P_{DVR}) for voltage sags and swells, considering a zero-phase angle jump:

$$P_{DVR} = \left(\frac{V_{pcc} - V_f}{V_{pcc}}\right) \cdot P_{load}\,, \tag{17}$$

where V_f is the voltage at terminals of voltage source converter in DVR; P_{load} is the active power consumed by load; V_{pcc} is the voltage at PCC.

Additionally, the Voltage Unbalance Factor (VUF) is assessed according to the standards set by the National Electrical Manufacturers Association is expressed as:

$$VUF(\%) = \frac{V_2}{V_1} \cdot 100\%\,, \tag{18}$$

where the positive sequence voltage V_1 and negative sequence voltage V_2 are considered, with phase angle δ between grid voltage V_g and terminal voltage of PMSG V_t needing to be kept below a specified maximum value to prevent overloading of DVR.

The given equation establishes the maximum allowable phase angle:

$$\delta_{\max} = \cos^{-1}\left(\frac{V_t^2 + V_g^2 - V_{c(\max)}^2}{2 \cdot V_d \cdot V_t}\right), \tag{19}$$

where $V_{c\max}$ is the maximum compensating voltage provided by DVR.

For enhancing performance of DVR the proposed work implements type 2 fuzzy controller, which ensures precise and adaptive regulation of voltage fluctuations and grid disturbances for seamless operation.

Type 2 fuzzy logic controller. T2-FLC is an advanced fuzzy logic system that handles uncertainties more effectively than traditional fuzzy controllers. In the context of DVR control, where power grid disturbances and uncertainties are prevalent, T2-FLC offers enhanced capabilities. The architecture of proposed T2-FLC is illustrated in Fig. 3.

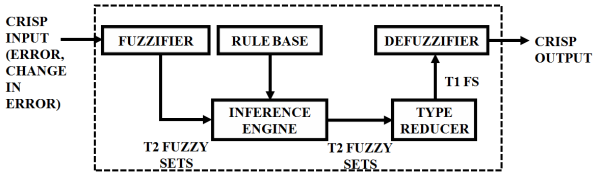

Fig. 3. Proposed structure of T2-FLC

Here's how type 2 fuzzy logic can be specifically applied for DVR control.

Fuzzification. Crisp input signals are generated by comparing the reference DC link voltage (expected stable voltage level) and the actual DC link voltage (measured voltage level during grid disturbances). These crisp inputs are fuzzified by T2-FLC into fuzzy variables using appropriate membership functions. The use of type 2 fuzzy sets allows the controller to handle uncertainties and variations effectively.

Rule base. The T2-FLC utilizes a set of fuzzy IF-THEN rules stored in the rule base. These rules capture the relationships between the fuzzy input variables. For instance, «IF Deviation is Negative Large AND Change in Deviation is Positive Small, THEN Control Signal is X». These rules encode the expert knowledge or system behavior and guide the inference process.

Inference engine. The inference engine applies FLC operations (such as AND, OR) on fuzzy input variables based on the fuzzy rules. This process results in fuzzy output sets that represent the intermediate control actions inferred from the inputs. In T2-FLC, additional operations are performed to handle uncertainties in the inference process, ensuring robust control decisions.

Table 2 illustrates generic example of fuzzy rules for a simplified scenario involving the control of DVR based on 2 input variables: «Error» (deviation between reference and actual DC link voltage) and «Change in Error» (rate of change of error).

Table 2

Fuzzy rule

Error	Change in error	Control signal
NL	*NL*	*NL*
NL	*NS*	*NM*
NL	*Z*	*NS*
NL	*PS*	*Z*
NL	*PL*	*PS*
NS	*NL*	*NM*
NS	*NS*	*NS*
NS	*Z*	*Z*
NS	*PS*	*PS*
NS	*PL*	*PM*

In Table 2 *NL*, *NS*, *NM* are negative large, negative small and negative medium, while *PL*, *PS*, *PM* are positive large, positive small and positive medium. Also *Z* indicates zero.

Type reducer. The output from the inference stage is a T2-fuzzy set, which contains more uncertainty than type-1 fuzzy sets. Type reduction is the process of converting the T2 fuzzy set into a more manageable T1-fuzzy set. It reduces the uncertainty associated with the control decisions, making them more reliable.

Defuzzification. Fuzzy output sets back into crisp control signals using defuzzification methods. This algorithm calculates the crisp control signals using the centroids and spreads of fuzzy output sets, ensuring precise and effective control actions.

Crisp output. The crisp control signals obtained after defuzzification represent the necessary actions the DVR system must take to restore voltage stability. These actions typically involve injecting compensating voltage into the distribution system through the transformer, effectively mitigating voltage sags or swells and ensuring that sensitive loads connected to the grid remain operational.

Thereby, the T2-FLC ensures precise and adaptive control actions, enabling DVR to effectively compensate for voltage fluctuations and maintain stable power supply.

Isolated flyback converter. The isolated flyback converter is shown in Fig. 4, it is a crucial component in the proposed system, designed to adjust voltage levels, ensure electrical isolation, and facilitate stable power transfer.

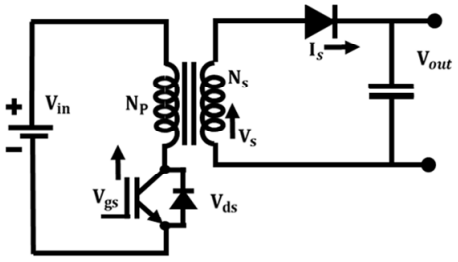

Fig. 4. Configuration of isolated flyback converter

In this intricate process, the converter receives regulated DC power from the PWM rectifier, which has previously converted unstable AC supply into a stable form. Operating in distinct switch-on and switch-off periods, the flyback converter employs a transformer to achieve electrical isolation. By precisely controlling the switch-on and switch-off periods, the flyback converter regulates output voltage, a crucial aspect for stable power transfer. The regulated DC output, now free from ripples, is subsequently rectified and filtered, ensuring a smooth waveform. Prominently, the flyback converter provides electrical isolation, safeguarding components from voltage spikes and disturbances in grid. Its efficient energy transfer, minimal power losses, and precise control, guided by signals from the PI controller at the grid side.

Reduced switch 31 level CHBMLI. The rectified output from WECS is processed through an isolated flyback converter before reaching the reduced switch 31-level CHBMLI. This converter ensures the adjustment of voltage levels and provides electrical isolation. The primary function of the 31-level CHBMLI is to convert the DC power from the isolated flyback converter into high-quality AC power.

The proposed configuration streamlines the design by reducing the number of DC source into single source, facilitated by the implementation of isolated flyback converter. The design of MLI is founded on H-bridge inverter, featuring a total 8 switches (Fig. 5). This design comprises a level generation unity and a polarity generation unit (H-bridge inverter). The switches associated with polarity generation (T_1 – T_4) and level generation (S_1 – S_4) collectively contribute to the generation of 31 voltage levels. The activation of switches T_1 and T_2 occur during positive half cycle, while T_3 and T_4 are engaged during the negative half cycle. Notably, the deactivation of all level generation switches yields the zero voltage level. This configuration allows for effective control and modulation of the output voltage levels, ensuring the desired multilevel characteristics of the inverter.

In positive half cycle, conduction occurs through D_2, D_3 and D_4 with switch S_1 turned ON. Table 3 presents the switching operations and corresponding output voltage levels during the operation of proposed system.

Transitioning to mode 2 in the positive half cycle, conduction shifts to D_1, D_3 and D_4 with switch S_2 turned ON, and yielding an output.

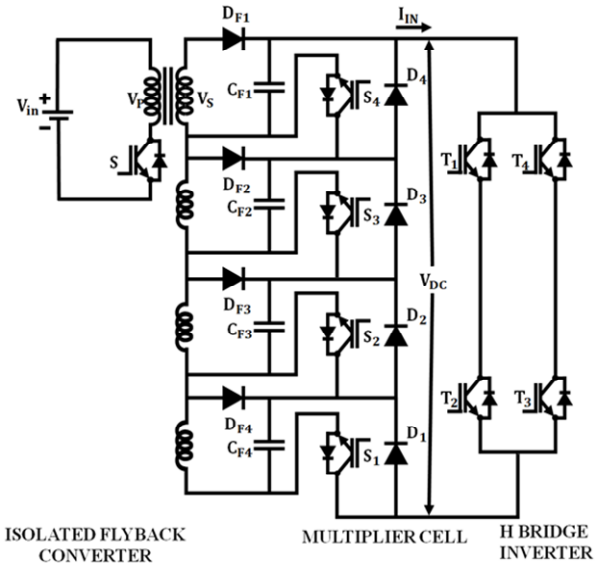

Fig. 5. Reduced switch 31-level MLI

Table 3

Switching operations and output voltage levels of reduced switch 31-level MLI

S_1	S_2	S_3	S_4	Output voltage
1	1	1	1	$V_{S1} + V_{S2} + V_{S3} + V_{S4}$
0	1	1	1	$V_{S2} + V_{S3} + V_{S4}$
1	0	1	1	$V_{S1} + V_{S3} + V_{S4}$
0	0	1	1	$V_{S3} + V_{S4}$
1	1	0	1	$V_{S1} + V_{S2} + V_{S4}$
0	1	0	1	$V_{S2} + V_{S4}$
1	0	0	1	$V_{S1} + V_{S4}$
0	0	0	1	V_{S4}
1	1	1	0	$V_{S1} + V_{S2} + V_{S3}$
0	1	1	0	$V_{S2} + V_{S3}$
1	0	1	0	$V_{S1} + V_{S3}$
0	0	1	0	V_{S3}
1	1	0	0	$V_{S1} + V_{S2}$
0	1	0	0	V_{S2}
1	0	0	0	V_{S1}
0	0	0	0	0
1	0	0	0	$-V_{S1}$
0	1	0	0	$-V_{S2}$
1	1	0	0	$-(V_{S1} + V_{S2})$
0	0	1	0	$-V_{S3}$
1	0	1	0	$-(V_{S1} + V_{S3})$
0	1	1	0	$-(V_{S2} + V_{S3})$
1	1	1	0	$-(V_{S1} + V_{S2} + V_{S3})$
0	0	0	1	$-V_{S4}$
1	0	0	1	$-(V_{S1} + V_{S4})$
0	1	0	1	$-(V_{S2} + V_{S4})$
1	1	0	1	$-(V_{S1} + V_{S2} + V_{S4})$
0	0	1	1	$-(V_{S3} + V_{S4})$
1	0	1	1	$-(V_{S1} + V_{S3} + V_{S4})$
0	1	1	1	$-(V_{S2} + V_{S3} + V_{S4})$
1	1	1	1	$-(V_{S1} + V_{S2} + V_{S3} + V_{S4})$

This sequential switching pattern continues through the 15 modes, with switches being activated in sequence. The same switching sequence is then repeated for negative half cycle. In addition, a PI controller is implemented for controlling the operation of 31-level CHBMLI. The PI controller continuously monitors real and reactive power, generating control signals for the inverter. This ensures precise control over the output voltage and current. This guarantees that the wind farm can seamlessly integrate with the grid without causing disruptions.

Table 3 enumerates the switching operations and associated output voltage levels for reduced switch 31-level MLI. Each row in the table corresponds to a specific switch configuration, where «1» indicates the switch is turned ON, and «0» denotes it is OFF. The switches are denoted as (S_1 – S_4). The output voltage column shows the cumulative voltage produced by the active switches according to the specified configuration. Columns (S_1 – S_4) represent the ON/OFF status of each switch in the inverter. Columns (V_{S1} – V_{S4}) specifies the resulting output voltage based on active switches. The notation (V_{S1} – V_{S4}) represents the voltage levels associated with each switch. The cumulative output voltage is calculated by adding the voltages of active switches. For example, the row «1 1 1 1» indicates that all 4 switches (S_1 – S_4) are turned ON, contributing their respective voltage levels to the total output voltage. In contrast, the row «0 0 0 0» signifies that none of the switches are active, resulting in zero output voltage. This table serves as a reference for understanding the relationship between switch configurations and the generated output voltage levels in the reduced switch 31-level MLI.

Result and discussion. The validation of proposed system has been precisely carried out using MATLAB simulation. Through rigorous analysis and simulation, the performance and effectiveness of each component within the system have been assessed. Table 4 presents a detailed breakdown of the specification parameters crucial to the design of the proposed system.

Table 4

Specification of design parameters

Parameters	Value
PMSG-wind system	
No. of turbines	1
Power, kW	10
Voltage, V	575
Stator resistance, Ω	0.975
Flux linkage, Wb	0.91
PMSG inductance, H	0.01
Pole pairs	3
Air density, kg/m^3	1.218
Pitch angle beta, degree	2
Base wind speed, m/s	12
DC link capacitor, μF	1500
DVR	
Switching frequency, kHz	10
Series voltage injection, V	100
Grid voltage, V	415
Filter inductance, mH	2.7
Filter capacitance, μF	50
Line resistance, Ω	0.1
Line inductance, mH	0.5

The following sections delve into the comprehensive results and discussions, shedding light on the system's response to grid disturbances, the role of DVR, and the overall enhancement of LVRT capability in PMSG based WECS.

Scenario 1. Voltage sag. The response of a PMSG during a voltage sag condition is illustrated in Fig. 6. Subfigures (*a*) and (*b*) respectively showcase the voltage and current waveforms of PMSG system under the influence of voltage sag. The occurrence is notable

between 0.2 s and 0.3 s, attributed to the uneven nature of the wind affecting the generator. The inphase waveform under voltage sag condition is depicted in Fig. 6,*c*. This visual representation enables a detailed observation of how PMSG system responds to voltage sag, offering valuable information about its dynamic characteristics in the presence of such adverse electrical conditions. The implementation of DVR plays a crucial role in mitigating voltage sag scenario.

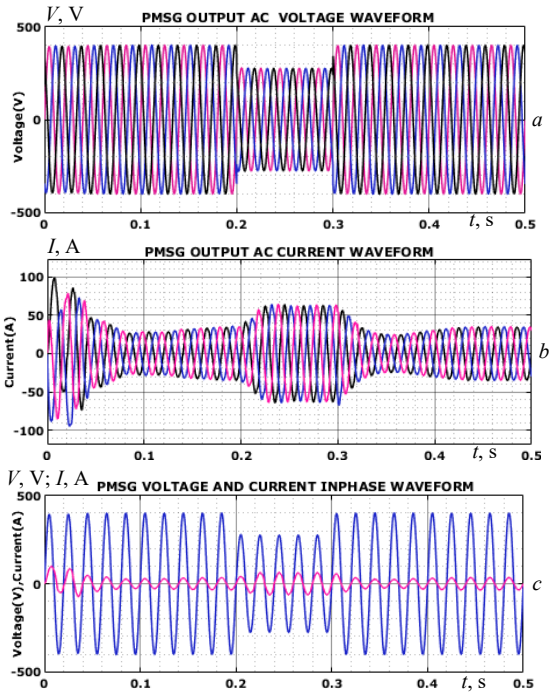

Fig. 6. PMSG behavior in voltage sag:
a – voltage; *b* – current; *c* – inphase waveforms

In Fig. 7, two key aspects of the system are depicted. Figure 7,*a* illustrates the output from the rectifier, displaying a gradual voltage increase with minor oscillations, indicating successful conversion of wind system power. Figure 7,*b* shows the stabilized DC link voltage at 800 V, highlighting a successful conversion and regulation process. This stable DC link voltage is essential for ensuring overall system performance and efficiency in subsequent stages.

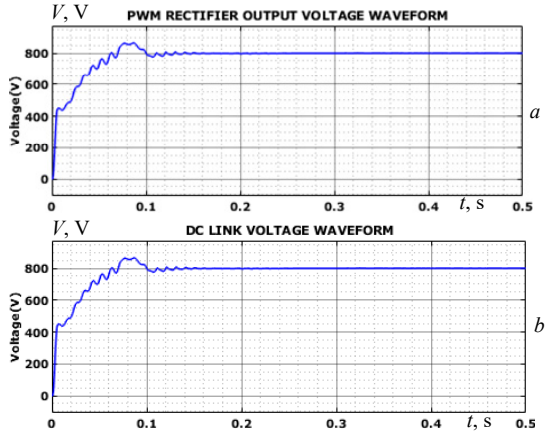

Fig. 7. *a* – output voltage from rectifier; *b* – voltage across DC link

In Fig. 8 the output characteristics of the 31-level MLI is shown. Figure 8,*a* illustrates the output voltage, showcasing a stabilized and consistent voltage profile. Concurrently, Fig. 8,*b* demonstrates the corresponding output current profile, which also maintains a stable and steady behavior. This stability in both voltage and current outputs highlights the efficacy of the 31-level MLI in providing a reliable and consistent power supply. The achieved output stability is crucial for ensuring the proper functioning of the connected load and contributes to the overall performance and efficiency of the system.

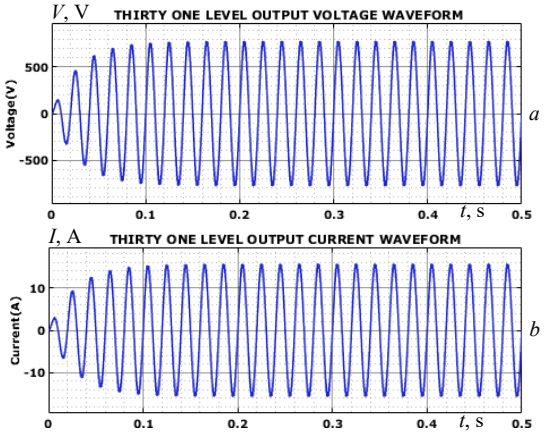

Fig. 8. Output voltage (*a*) and current (*b*) profile of 31 level MLI

Figure 9 provides a visual representation of the voltage and current characteristics in 3 phase grid load under the influence of proposed system. Figure 9,*a* displays the load voltage waveform, showcasing the stabilized nature of voltage. This stabilization is a result of proposed system's effective mitigation of voltage sag issues, ensuring a consistent and reliable voltage supply to the grid load. Simultaneously, Fig. 9,*b* illustrates the load current waveform, indicating a stabilized current value. The ability to maintain stable voltage and current levels is crucial for the overall performance and reliability of the grid load, emphasizing positive impact of proposed system on mitigating voltage sag and ensuring the steady operation of grid load.

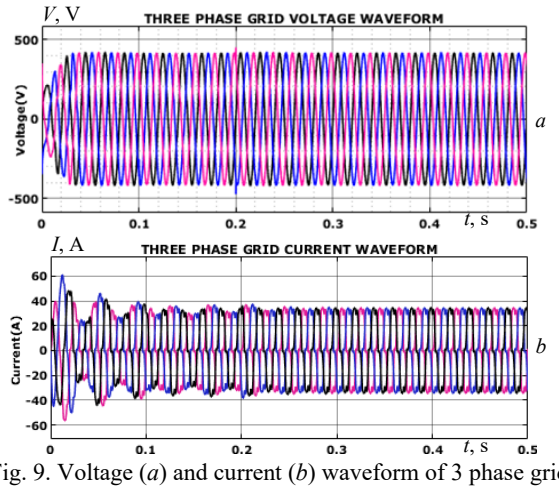

Fig. 9. Voltage (*a*) and current (*b*) waveform of 3 phase grid

Figure 10 illustrates the dynamics of both real and reactive power waveforms, providing insights into the power characteristics of proposed system under operating conditions. The real power waveform represents the actual power consumed by the system, while the reactive power waveform indicates system's ability to maintain voltage levels. Together, these waveforms offer a

comprehensive view of the power behavior of the system, aiding in the evaluation of its performance and efficiency.

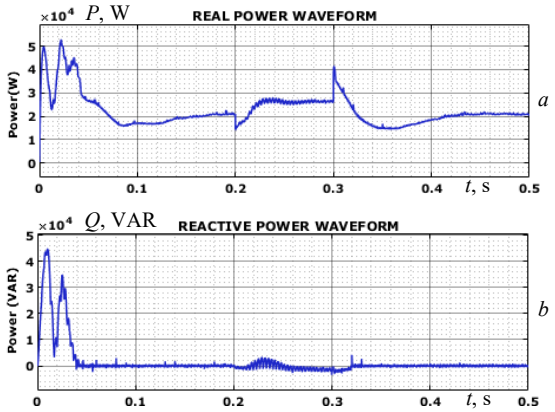

Fig. 10. Real (*a*) and reactive (*b*) power waveform

Scenario 2. Voltage swell. The response of PMSG system under voltage swell conditions is shown in Fig. 11. Figure 11,*a* illustrates the voltage waveform, showcasing how the system's voltage output is affected by voltage swell condition between 0.2 – 0.3 s. In parallel, Fig. 11,*b* details the corresponding current waveform, providing insights into the system's electrical behavior in response to the voltage swell. Additionally, the inphase representation of current and voltage is also revealed in Fig. 11,*c*.

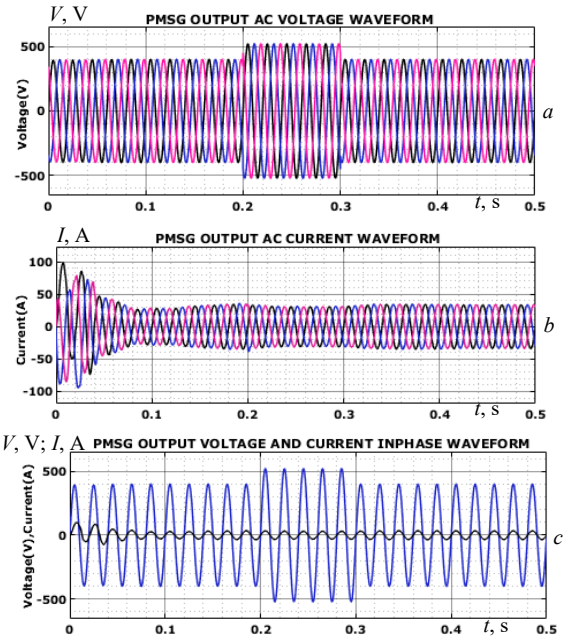

Fig. 11. PMSG system response to voltage swell: *a* – voltage; *b* – current; *c* – inphase waveform

In Fig. 12, two essential elements of the system are depicted: output from rectifier and the resulting DC link voltage. Figure 12,*a* illustrates the rectifier's output, displaying a gradual voltage increase with minor oscillations. This highlights the rectifier's role in converting wind system input power into a usable form. Figure 12,*b* shows the DC link voltage, indicating a stabilized output at 800 V. This successful conversion and regulation process ensures a consistent and reliable DC supply for the subsequent stages of the system, contributing to overall performance and efficiency.

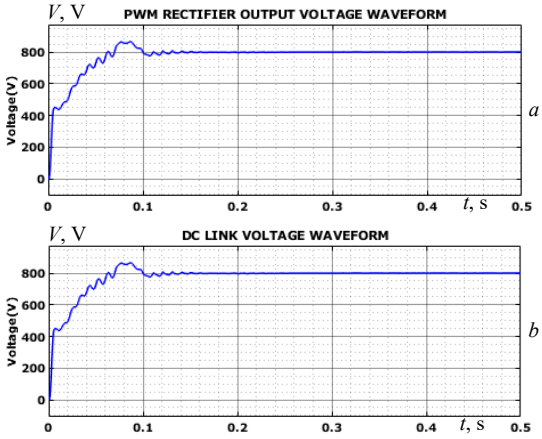

Fig. 12. Rectifier output voltage (*a*) and DC link voltage (*b*)

In Fig. 13, the output voltage and current profiles of 31-level MLI under voltage swell conditions are depicted. Figure 13,*a* illustrates the stabilized output voltage, emphasizing system's ability to mitigate the effects of voltage swell and maintain a consistent voltage supply. Simultaneously, Fig. 13,*b* presents the corresponding output current profile, showcasing the system's capability to deliver stable current despite the voltage variations. This analysis underscores the effectiveness of the proposed system in adapting to both voltage sag and swell conditions and ensuring reliable power delivery to connected load.

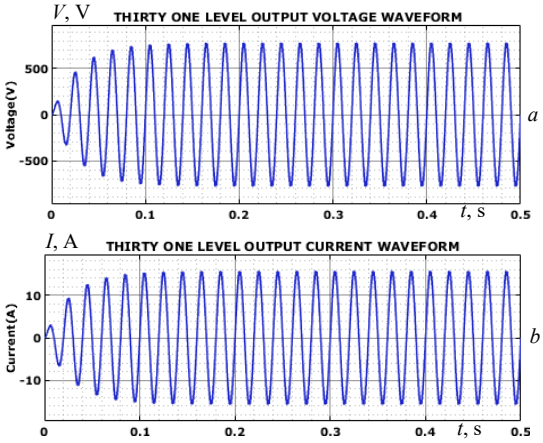

Fig. 13. *a* – stabilized output voltage; *b* – consistent output current profile of 31-level MLI under voltage swell condition

The voltage and current dynamics within 3 phase grid load influenced by the proposed system is depicted in Fig. 14. Figure 14,*a* depicts the load voltage waveform, demonstrating the system's proficiency in stabilizing voltage by effectively addressing voltage swell issues. Concurrently, Fig. 14,*b* portrays the load current waveform, showcasing a steady and controlled current level. The system's capability to maintain stability in both voltage and current is instrumental for the reliable performance of grid load, underscoring the positive impact of the proposed solution in mitigating voltage swell and ensuring uninterrupted operation of grid load.

The concise view of power dynamics, encompassing both real and reactive power waveforms is illustrated in Fig. 15. Figure 15,*a* represents the real power waveform, reflecting the actual power consumed. Simultaneously, Fig. 15,*b* depicts the reactive power waveform, indicating

the non-working power component that oscillates between source and load. This comprehensive representation of real and reactive power dynamics is crucial for assessing the system's performance and efficiency in delivering power to the connected load.

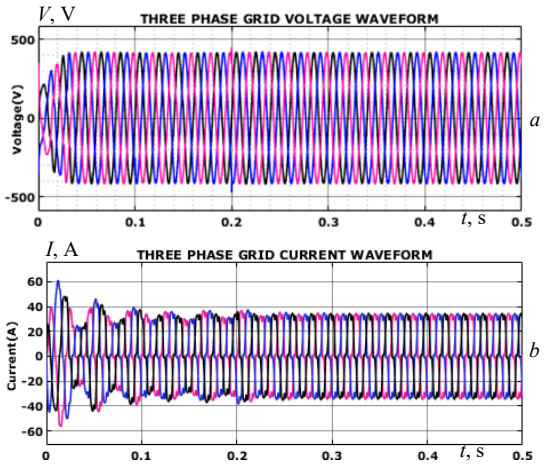

Fig. 14. Voltage (*a*) and current (*b*) waveform of 3 phase grid

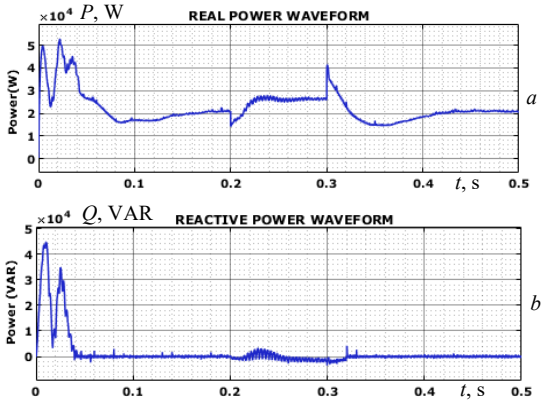

Fig. 15. Real (*a*) and reactive (*b*) power waveform

The power factor waveform accomplished by the proposed system is illustrated in Fig. 16. The achieved unity power factor signifies optimal utilization and balance between real and reactive power, showcasing the efficiency and stability of the system under voltage swell conditions. The consistent power factor dynamics affirm the system's capability to maintain a balanced and reliable operation even in challenging scenarios.

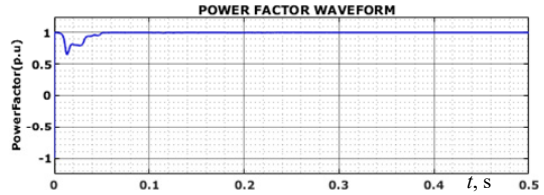

Fig. 16. Power factor dynamics

Figure 17 presents the THD value, which is recorded at 1.8 %. This low THD value indicates a minimal level of harmonic distortion in the system's output, highlighting the efficiency and quality of the power signal generated by the proposed configuration.

A comprehensive comparison of THD analysis among various techniques is listed in Table 5. The table serves as a valuable reference for evaluating and contrasting the harmonic distortion levels achieved by different approaches, with the lower THD values indicating better performance in terms of generating a cleaner and more stable power output.

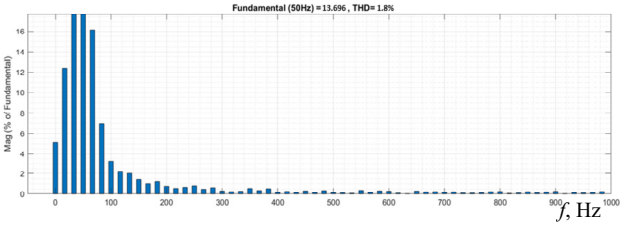

Fig. 17. THD waveform

From Table 5, the first three rows represent the THD percentages reported by different authors, specifically Pal R. [24], Moghassemi A. [25], and Ibrahim N.F. [26], revealing THD value of 7.85 %, 4.89 % and 2.3 % respectively. While, the proposed technique included in the comparison, shows a reduced THD value of 1.8 %, with optimal performance.

Table 5

Comparison of THD analysis

Techniques	THD (%)
Pal R. [24]	7.85
Moghassemi A. [25]	4.89
Ibrahim N.F. [26]	2.3
Proposed	1.8

The comparison of cost function between a fuzzy controller and a T2-FLC for optimal DVR control is illustrated in Fig. 18. The analysis reveals that T2-FLC outperforms traditional fuzzy controller, achieving a minimized cost. Figure 18 provides valuable insights into the effectiveness of T2-FLC controller in optimizing DVR control and reducing associated costs, showcasing its superiority over conventional fuzzy control strategies.

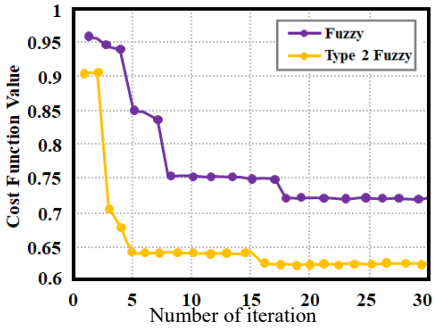

Fig. 18. Comparison of cost function

A comparative analysis of convergence speed between fuzzy controller and T2-FLC controller is represented in Fig. 19. The comparison highlights the enhanced convergence speed achieved by type 2 fuzzy controller, showcasing its greater performance in optimizing convergence dynamics compared to conventional fuzzy. Figure 19 provides valuable insights into the efficiency and effectiveness of type 2 fuzzy controller in ensuring faster convergence for improved control outcomes.

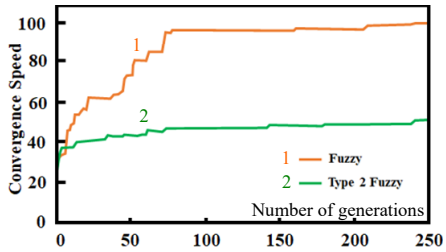

Fig. 19. Comparison of convergence speed

Figure 20 illustrates a comprehensive comparison of DVR controller errors. This analysis examines and contrasts the errors associated with different control strategies employed for the DVR system. It observed that the proposed type 2 fuzzy shed light on accuracy and efficacy of each control approach in minimizing errors within the DVR system in contrast to fuzzy approach.

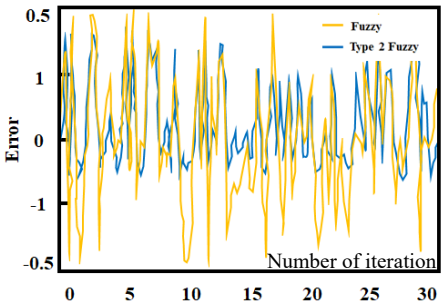

Fig. 20. DVR controller error comparison

Conclusions. In conclusion, the proposed integration of PMSG-WECS with an advanced power conditioning system, including a DVR represents a significant advancement in enhancing grid stability and LVRT capability. The type 2 fuzzy controller intelligently regulates the input DC voltage to DVR, adapting dynamically to changing conditions and tackling voltage fluctuations and grid disturbances. The subsequent processing of rectified WECS output through an isolated flyback converter and a 31-level CHBMLI with PI control ensures the delivery of high-quality AC output to grid, minimizing harmonics and voltage deviations. This holistic approach significantly improves the WECS's LVRT capability with reduced THD value of 1.8 %, providing a cleaner and more stable power output compared to existing techniques. The comprehensive comparison of THD analysis with other techniques and the examination of controller errors affirm the scientific novelty and effectiveness of the proposed system. In conclusion, the research not only addresses the stated research problem but also contributes novel insights into the integration of RES into the power grid, emphasizing the significance of advanced control strategies, such as type 2 fuzzy control, in improving the system's consistency. To raise the overall resilience and efficiency of the system, future work will concentrate on modified controllers for even more adaptability, scaling up and optimizing the suggested PMSG-WECS integration, and investigating new developments in energy storage technologies.

Conflict of interest. The authors declare that they have no conflicts of interest.

REFERENCES

1. Zhou A., Li Y.W., Mohamed Y. Mechanical Stress Comparison of PMSG Wind Turbine LVRT Methods. *IEEE Transactions on Energy Conversion*, 2021, vol. 36, no. 2, pp. 682-692. doi: https://doi.org/10.1109/TEC.2020.3018093.

2. Chojaa H., Derouich A., Zamzoum O., Watil A., Taoussi M., Abdelaziz A.Y., Elbarbary Z.M.S., Mossa M.A. Robust Control of DFIG-Based WECS Integrating an Energy Storage System With Intelligent MPPT Under a Real Wind Profile. *IEEE Access*, 2023, vol. 11, pp. 90065-90083. doi: https://doi.org/10.1109/ACCESS.2023.3306722.

3. Bouraghda S., Sebaa K., Bechouat M., Sedraoui M. An improved sliding mode control for reduction of harmonic currents in grid system connected with a wind turbine equipped by a doubly-fed induction generator. *Electrical Engineering & Electromechanics*, 2022, no. 2, pp. 47-55. doi: https://doi.org/10.20998/2074-272X.2022.2.08.

4. Kim C., Kim W. Low-Voltage Ride-Through Coordinated Control for PMSG Wind Turbines Using De-Loaded Operation. *IEEE Access*, 2021, vol. 9, pp. 66599-66606. doi: https://doi.org/10.1109/ACCESS.2021.3076787.

5. Khan A., Ahmad H., Ahsan S.M., Gulzar M.M., Murawwat S. Coordinated LVRT Support for a PMSG-Based Wind Energy Conversion System Integrated into a Weak AC-Grid. *Energies*, 2021, vol. 14, no. 20, art. no. 6588. doi: https://doi.org/10.3390/en14206588.

6. Yuan L., Meng K., Huang J., Dong Z.Y., Zhang W., Xie X. Development of HVRT and LVRT Control Strategy for PMSG-Based Wind Turbine Generators. *Energies*, 2020, vol. 13, no. 20, art. no. 5442. https://doi.org/10.3390/en13205442.

7. Kim C., Kim W. Enhanced Low-Voltage Ride-Through Coordinated Control for PMSG Wind Turbines and Energy Storage Systems Considering Pitch and Inertia Response. *IEEE Access*, 2020, vol. 8, pp. 212557-212567. doi: https://doi.org/10.1109/ACCESS.2020.3040905.

8. Desalegn B., Gebeyehu D., Tamrat B. Smoothing electric power production with DFIG-based wind energy conversion technology by employing hybrid controller model. *Energy Reports*, 2023, vol. 10, pp. 38-60. doi: https://doi.org/10.1016/j.egyr.2023.06.004.

9. Ghanem S., Fandi G., Kyncl J., Müller Z. A novel scheme for control by active and reactive power utilized in gearless variable speed wind turbine system with PMSG connected to the grid. *Electrical Engineering & Electromechanics*, 2022, no. 2, pp. 56-68. doi: https://doi.org/10.20998/2074-272X.2022.2.09.

10. Döşoğlu M.K., Güvenç U., Sönmez Y., Yılmaz C. Enhancement of demagnetization control for low-voltage ride-through capability in DFIG-based wind farm. *Electrical Engineering*, 2018, vol. 100, no. 2, pp. 491-498. doi: https://doi.org/10.1007/s00202-017-0522-6.

11. Zhang A., Chen Z., Gao R., Wang J., Ma Z., Wang S., Wang Y. Crowbarless Symmetrical Low-Voltage Ride Through Based on Flux Linkage Tracking For Brushless Doubly Fed Induction Generators. *IEEE Transactions on Industrial Electronics*, 2020, vol. 67, no. 9, pp. 7606-7616. doi: https://doi.org/10.1109/TIE.2019.2944096.

12. Chowdhury M.A., Shafiullah G.M., Ferdous S.M. Low voltage ride-through augmentation of DFIG wind turbines by simultaneous control of back-to-back converter using partial feedback linearization technique. *International Journal of Electrical Power & Energy Systems*, 2023, vol. 153, art. no. 109394. doi: https://doi.org/10.1016/j.ijepes.2023.109394.

13. Liu J., Zhao C., Xie Z. Power and Current Limiting Control of Wind Turbines Based on PMSG Under Unbalanced Grid Voltage. *IEEE Access*, 2021, vol. 9, pp. 9873-9883. doi: https://doi.org/10.1109/ACCESS.2021.3049839.

14. Jayasawal K., Thapa K. An Enhanced Low Voltage Ride-Through Control Scheme of a DIFG based WTG Using Crowbar and Braking Chopper. *Journal of the Institute of Engineering*, 2021, vol. 16, no. 1, pp. 61-67. doi: https://doi.org/10.3126/jie.v16i1.36537.

15. Gontijo G.F., Tricarico T.C., da Silva L.F., Krejci D., Franca B.W., Aredes M., Guerrero J.M. Modeling, Control, and Experimental Verification of a DFIG With a Series-Grid-Side Converter With Voltage Sag, Unbalance, and Distortion Compensation Capabilities. *IEEE Transactions on Industry Applications*, 2020, vol. 56, no. 1, pp. 584-600. doi: https://doi.org/10.1109/TIA.2019.2946950.

16. Labed M.A., Zellagui M., Benidir M., Sekhane H., Tebbakh N. Optimal hybrid photovoltaic distributed generation and distribution static synchronous compensators planning to minimize active power losses using adaptive acceleration

coefficients particle swarm optimization algorithms. *Electrical Engineering & Electromechanics*, 2023, no. 6, pp. 84-90. doi: https://doi.org/10.20998/2074-272X.2023.6.15.
17. Rezaie H., Kazemi-Rahbar M.H. Enhancing voltage stability and LVRT capability of a wind-integrated power system using a fuzzy-based SVC. *Engineering Science and Technology, an International Journal*, 2019, vol. 22, no. 3, pp. 827-839. doi: https://doi.org/10.1016/j.jestch.2018.12.018.
18. Zahra S.T., Khan R.U., Ullah M.F., Begum B., Anwar N. Simulation-based analysis of dynamic voltage restorer with sliding mode controller at optimal voltage for power quality enhancement in distribution system. *Electrical Engineering & Electromechanics*, 2022, no. 1, pp. 64-69. doi: https://doi.org/10.20998/2074-272X.2022.1.09.
19. Zhu Y., Wang Z., Guo X., Wei Z. An improved kinetic energy control strategy for power smoothing of PMSG-WECS based on low pass filter and fuzzy logic controller. *Electric Power Systems Research*, 2023, vol. 214, art. no. 108816. doi: https://doi.org/10.1016/j.epsr.2022.108816.
20. Nguyen Huy T., Le Hanh D., Takano H., Nguyen Duc T. Cooperative LVRT control for protecting PMSG-based WTGs using battery energy storage system. *Energy Reports*, 2023, vol. 9, pp. 590-598. doi: https://doi.org/10.1016/j.egyr.2023.05.112.
21. Abas N., Dilshad S., Khalid A., Saleem M.S., Khan N. Power Quality Improvement Using Dynamic Voltage Restorer. *IEEE Access*, 2020, vol. 8, pp. 164325-164339. https://doi.org/10.1109/ACCESS.2020.3022477.
22. Appala Naidu T., Arya S.R., Maurya R., Padmanaban S. Performance of DVR Using Optimized PI Controller Based Gradient Adaptive Variable Step LMS Control Algorithm. *IEEE Journal of Emerging and Selected Topics in Industrial Electronics*, 2021, vol. 2, no. 2, pp. 155-163. doi: https://doi.org/10.1109/JESTIE.2021.3051553.
23. Kumar P., Arya S.R., Mistry K.D., Yadav S. A self-tuning ANFIS DC link and ANN-LM controller based DVR for power quality enhancement. *CPSS Transactions on Power Electronics and Applications*, 2023, vol. 8, no. 4, pp. 424-436. doi: https://doi.org/10.24295/CPSSTPEA.2023.00032.
24. Pal R., Gupta S. Topologies and Control Strategies Implicated in Dynamic Voltage Restorer (DVR) for Power Quality Improvement. *Iranian Journal of Science and Technology, Transactions of Electrical Engineering*, 2020, vol. 44, no. 2, pp. 581-603. doi: https://doi.org/10.1007/s40998-019-00287-3.
25. Moghassemi A., Ebrahimi S., Ferdowsi F. A Novel Control Scheme for TransZSI-DVR to Enhance Power Quality in Solar Integrated Networks. *2021 North American Power Symposium (NAPS)*, 2021, pp. 1-6. doi: https://doi.org/10.1109/NAPS52732.2021.9654507.
26. Ibrahim N.F., Alkuhayli A., Beroual A., Khaled U., Mahmoud M.M. Enhancing the Functionality of a Grid-Connected Photovoltaic System in a Distant Egyptian Region Using an Optimized Dynamic Voltage Restorer: Application of Artificial Rabbits Optimization. *Sensors*, 2023, vol. 23, no. 16, art. no. 7146. doi: https://doi.org/10.3390/s23167146.

Received 07.01.2024
Accepted 14.03.2024
Published 20.06.2024

Ch. Sajan[1], *Research Scholar*,
P. Satish Kumar[1], *Professor*,
P. Virtic[2], *Professor*,
[1] Department of Electrical Engineering,
University College of Engineering, Osmania University,
Hyderabad, Telangana 500007, India,
e-mail: sajan4315@gmail.com (Corresponding Author);
satish_8020@yahoo.co.in
[2] Faculty of Energy Technology,
University of Maribor, Krško, Slovenia,
e-mail: peter.virtic@um.si

How to cite this article:
Sajan Ch., Satish Kumar P., Virtic P. Enhancing grid stability and low voltage ride through capability using type 2 fuzzy controlled dynamic voltage restorer. *Electrical Engineering & Electromechanics*, 2024, no. 4, pp. 31-41. doi: https://doi.org/10.20998/2074-272X.2024.4.04